

Boron Neutron Capture Therapy of MCF-7 Breast Cancer Cells by Using Calcium Fructoborate@Au Nanoparticles Drug Encapsulated in Liposomal Nanocarriers: *In-vitro* Experimental Investigation

Meisam Sadeghi^{1*}, Zahra Moghimifar² and Hamedreza Javadian²

¹Nanotechnology Research Institute, Faculty of Chemical Engineering, Babol Noshirvani University of Technology, Babol, Iran

²Chemistry & Chemical Engineering Research Center of Iran (CCERCI), P.O. Box 14335-186, Tehran, Iran

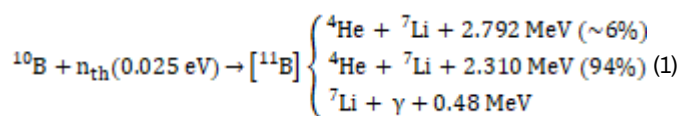
Abstract

In this research, calcium fructoborate (CFB) complex containing enriched ¹⁰B was used as a drug. The liposome prepared from phosphatidylcholine was applied as a biological macromolecule carrier of the drug. The liposome-encapsulated CFB (LECFB) was applied to treat MCF-7 breast cancer cells. The study demonstrated that AuNPs added to LECFB in the core-shell structure of LECFB with AuNPs (LECFB@AuNPs) can be considered selectively for the specific biological labeling and delivery of large quantities of boron to the cancer cells, respectively. Polyethylene glycol (PEG) and folic acid (FA) were chosen as appropriate substrates to potentially attach to folate receptors (FR) on the surface of cancer cells before liposomal formulation. The size of folate-conjugated LECFB@AuNPs was around 240.9 nm, while the size of synthesized LECFB was 142.3 nm. The optimum encapsulation efficiency was 72.38 ± 1.68% under the conditions of T=60°C, drug:lipid ratio=1:5, and incubation time=60 min. PEGylated liposome improved 0.07 mg of the drug loading content, and the amounts of the drug release from PEGylated formulation at 37 and 42 °C were respectively 8.89 and 5.78% more than those obtained by the optimum formula of the drug encapsulation.

Keywords: Boron neutron capture therapy • Liposome • Calcium fructoborate • MCF-7 cancer cells • Drug delivery

Introduction

BNCT is an effective treatment that uses compounds containing ¹⁰B to selectively destroy cancer cells without any influence on normal cells by a cell-by-cell basis technique [1], and it is proposed to clinically treat cancer cells [2]. In this method, the cancer cells are selectively destroyed using alpha and lithium particles that are generated by ¹⁰B(n,α)⁷Li reaction [3]. This reaction is demonstrated as follows:



Undoubtedly, a highly effective boron aggregation system should be designed in the initial step to significantly increase the successful absorption of boron-containing agents for use in the clinical aspect of the BNCT method. The effective delivery of drugs with liposomes as carriers for the selective transfer of a broad range of ¹⁰B agents to tumor tissues has been confirmed [4,5]. Indeed, liposomes are small bubbles with phospholipid bilayers that are surrounded and filled by water and a nano-drug, respectively. Therefore, liposomal encapsulation technology (LET) is applied for the entrapment of nano-drug [6,7] that is a highly effective method to raise the absorption

***Address for Correspondence:** Meisam Sadeghi, Nanotechnology Research Institute, Faculty of Chemical Engineering, Babol Noshirvani University of Technology, Babol, Iran, E-mail: meisam_sadeghi1363@yahoo.com

Copyright: © 2022 Sadeghi M, et al. This is an open-access article distributed under the terms of the Creative Commons Attribution License, which permits unrestricted use, distribution, and reproduction in any medium, provided the original author and source are credited

Date of Submission: 26 July, 2022, Manuscript No. jnmrt-22-70288; **Editor Assigned:** 30 July, 2022, PreQC No. P- 70288; **Reviewed:** 09 August, 2022, QC No. Q-70288; **Revised:** 16 August, 2022, Manuscript No. R-70288; **Published:** 21 August, 2022, DOI: 10.37421/2155-9619.2022.13.496.

efficiency of agents containing boron, and it represents a potential approach for the delivery of carrier systems [8].

Studies on these nanostructures have demonstrated them as efficient carriers for the study of drug release in the human body, in which the encapsulation of active content into a liposome has been done for the improvement of delivery, protection, bioavailability, and absorption [9]. Therefore, due to the results of thermal and elemental analyses [10,11], CFB was selected as a targeted boron-containing nano-drug, and liposome was considered as an appropriate substrate for the drug carrier [12,13]. Since noble metal nanoparticles tolerate phototoxicity and photobleaching [14,15], AuNPs as an attractive imaging agent are considered for specific biological labeling [16,17]. Accordingly, LECFB@AuNPs core-shell nanostructure as an efficient boronated nano-drug carrier could be more favorable for imaging due to their highly controlled optical properties [18].

Due to the low specification of antitumors, a limited number of antitumor agents are used for cancer treatment [19,20]. Folate-linked phospholipids (in the majority), peptides, and cholesterol can bind FR as tumor-associated antigen to FA conjugate with high affinity [21,22]. To develop drug carrier systems containing boron, FA and PEG have been considered as appropriate ligands with potential attachment to FR on the surface of cancer cells compared with several normal cells [23-25]. Lee, et al. have shown that a PEG spacer can be utilized to conjugate FA to the phospholipids to increase solubility, prolong the drug's half-life in the body, and increase the retention of liposomes and the accumulation of the drug at the site of the tumor [26]. This precise and efficient method facilitates drug absorption via endocytosis mediated with FR and enables targeting tumors overexpressed with FR [27-33]. Liposomes conjugated with folate have shown much higher cell death results for MCF-7 and PC-3 cells than conventional liposomes [34,35]. The MCF-7 cell line used in this research was a prominent sample of breast cancer cells isolated in 1970 from a 69-year-old Caucasian woman.

Recently, PEGylated liposomes have been used as a delivery vehicle for both hydrophilic and hydrophobic drugs. Some advantages of the encapsulation of CFB in nanoliposomes are as follows:

- Low toxicity
- Low unwanted side effects and
- Higher drug encapsulation efficiency [36].

In addition, the synthetic procedure of LECFB@AuNPs using PEG permits the binding of a ligand to the liposome and solubility of the drug in the blood [37]. Phosphatidylcholine is a liposome, in which the membrane of phospholipid is similar to the cell membranes in the body [38,39]. LECFB@AuNPs system designed for carrying and targeted release of CFB could be intelligent around cancer cells. Indeed, LECFB@AuNPs could absorb a defined light wavelength and transform optical energy into heat. These phenomena could induce a phase transition and release of the drug [40,41]. Given an adequate number of ^{10}B atoms (around 109 atoms/cell) that could selectively be delivered to the cancer cells, neutron beams could be absorbed by the cancer cells to maintain $^{10}\text{B}(n,\phi)^7\text{Li}$ reactions. Therefore, neutrons are radiated to the part of the cancer cells affected through neutron reactions. High-energy neutrons generated by $^{10}\text{B}(n,\phi)^7\text{Li}$ reactions over time could be able to damage and degrade the boron-containing cancer cells [42]. The entrance of boron into cancer cells is not carried out easily owing to the function of the cancer cells while it finds readily its way to enter the healthy cells [43-49]. In this method, the great challenge is the entrance of ^{10}B into cancer cells while the final target is a novel and promising approach for the improvement of the quality, performance, and efficiency of clinical treatment. Indeed, LECFB@AuNPs could be considered as a novel drug carrier enriched with large quantities of boron to treat cancer cells particularly.

The aim of this research was to report the effectiveness of appropriate encapsulation of CFB into PEGylated liposome for the treatment of MCF-7 breast cancer cells. Firstly, the characterization of the molecular composition of CFB was carried out using

Fourier transform infrared (FT-IR) spectroscopy and Raman analysis. Then, the LECFB@AuNPs as a carrier for imaging the BNCT process by fluorescence lifetime imaging was assessed owing to the capability of this nano vehicle to deliver boron compound.

Materials and Methods

Materials and instruments

PEGylated phosphatidylcholine liposome (Mw=2000 g/mol), PEG with the molecular weights of 2000 Da and 3350 Da as sources for short and long chains, respectively, folic acid and folate receptor alpha ($\text{FR}\alpha$), phosphate-buffered saline (PBS), and chloroauric acid (HAuCl_4) were bought from Sigma-Aldrich. Boric acid- ^{10}B was purchased from Daejung and D-fructose, CaCO_3 , and acetone were purchased from Merck. The materials and solvents were of reagent grade. In addition, Pasteur Institute, Tehran, Iran, has provided the MCF-7 breast cancer cell line. FT-IR and Raman spectra were respectively recorded using FT-IR-6300, JASCO International Company, Japan and thermo Nicolet Omega XR Dispersive Raman Spectrometer. A Dual Scope atomic force microscope (DME Danish Micro Engineering A/S, Denmark) in tapping mode was utilized. In addition, the particle size of the materials was measured by Particle Metrix, PMX 200CS (Germany). UV/Visible data were also obtained by UV160 Shimadzu, Japan.

Synthesis of CFB

CFB synthesis was carried out following the Miljkovic procedure. One popular strategy proposed for the synthesis of such high drug loading nanomedicines is to conjugate drug molecules with polymers. Briefly, 10 mL of distilled water was used to dissolve D-fructose, and boric acid- ^{10}B and calcium carbonate were then added to this solution to synthesize CFB that was then encapsulated in PEGylated liposome for the synthesis of LECFB. Two different isomeric structures of CFB are illustrated in Figure 1a and 1b.

Synthesis of folic acid-PEGylated liposome

The conjugation of FA to the liposome by means of PEG as a linker was

performed as follows: Initially, the synthesis of 100 mg of PEG-liposome was carried out. A primary amine was grafted to the termini of the chains of PEG by the addition of 1 mL of ethylenediamine to the suspension of liposome under the N_2 atmosphere. The sonication of the mixture was performed for 4 h at 60°C . Washing the amine-PEG-liposome with ethanol and anhydrous dimethyl sulfoxide (DMSO, 50 mL) was done three times. Then, linking the amino termini of PEG chains to FA was carried out chemically by the addition of 10 mL of pyridine to the liposome solution and 50 mL of 23 mM FA to DMSO with equimolar dicyclohexylcarbodiimide. The resulting mixture was reacted overnight on a shaker at 180 rpm while protected from light. The liposome conjugated with FA was washed twice with ethanol and sodium citrate (20 mM) at pH=8.0 and suspended again. The structure schematic of PEG-FA conjugate is shown in Figure 1c.

Encapsulation of CFB into the liposome and plot of the calibration curve

The most common liposome for medical applications is phosphatidylcholine. In the meantime, adding PEG to liposomes increases their circulation lifetime. When FA is conjugated to a longer chain of PEG (here, Mw=3350 Da), liposome interaction with targeted cells enhances compared with a short chain of PEG (here, Mw=2000 Da) that is commonly used for liposome conjugation. These insights can be concluded that folate ligand attached to large PEG are not repulsed when binding to their respective receptors at the cell surface. The encapsulation of CFB into the liposome was carried out following the procedure mentioned by Pirouz, et al. [50]. In order to plot the drug calibration curve, different concentrations of CFB drug were made in phosphate buffer by the standard series method. Then, their optical absorbance by the spectrophotometer was recorded, and finally, the calibration curve, line equation, and coefficient of determination were calculated.

Specific biological labeling using LECFB@AuNPs

AuNPs synthesized by reducing Au ions with citric acid were used for clinical application due to their optical and photothermal properties. Consequently, the complex of LECFB@AuNPs was synthesized by adding AuNPs to the liposome suspension in PBS buffer solution and then stirring with a vortex. Since AuNPs are conjugated effectively with PEG (Au-PEG-LECFB), they cause a successful delivery of CFB to the MCF-7 breast cancer cells. It should be noted that AuNPs bond to the shorter length of the PEG chain. The schematic of LECFB@AuNPs is demonstrated in Figure 1d. The efficient use of drugs requires their selective delivery and release to selected tumor sites at a controlled rate. To deliver and release nanoparticles at cellular levels to the whole body of BALB/C mice, there exist significant challenges [51]. For instance, assessing in-vivo in the models of preclinical animals has demonstrated that circulation lifetimes have been short and the accumulation of particles has been slight at the cancerous site. In addition, for X-ray imaging in RPMI-1640 cell culture, AuNPs as a contrast agent provide an enhancement in therapeutics because the particles are delivered successfully to the site of the tumor and internalized into the tumor cells. In this study, AuNPs shells were

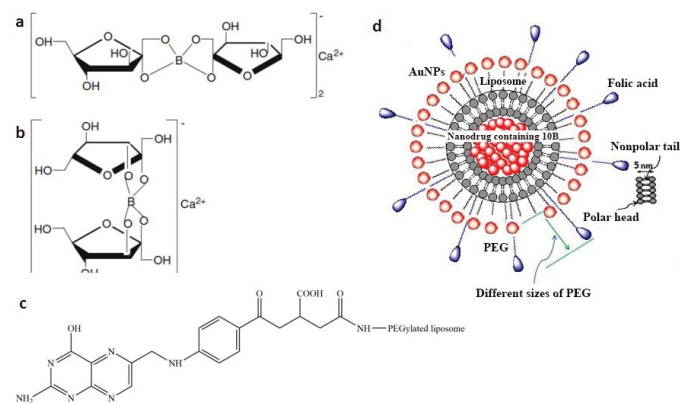


Figure 1. Different isotopes of CFB drug: (a) calcium α -D-fructofuranose borate, (b) Calcium β -D-fructofuranose borate, (c) Structure of FA and its binding to PEG and (d) Schematic of LECFB@AuNPs.

30–40 nm. All AuNPs could bind to PEG chains, and the binding could keep the stealth function of the PEGylated liposome.

Loading, smart delivery, and release of CFB

Optimization of CFB loading into the liposome: The encapsulation of CFB was performed at two conditions of temperature and time and different ratios of drug to lipid, and the best condition was obtained for the highest drug loading. Thus, the experiment was performed for 30 and 60 min at 60 and 70°C with the ratios of 1:5 and 1:10 for the drug to lipid (Table 1).

Determination of CFB encapsulation efficiency into the liposome: To determine the encapsulation efficiency of the drug, the liposomes were placed into the dialyzed bags and titrated for 1 h with different buffer volumes. The samples were placed at 4°C to release the free and unloaded drug. Then, liposomes made with liposome:PBS ratios of 1:10, 1:20, and 1:50 were mixed with sodium phosphate to break the surrounding lipid wall and release the drug. In the next step, the amount of absorption of the trapped drug was calculated using the spectrophotometer at the maximum wavelength. Finally, the rate of drug encapsulation into the liposome nanocarrier was calculated by using the standard calibration curve of CFB drug and the following equation:

$$\text{Encapsulation efficiency (\%)} = \frac{\text{Mass of drug in the liposome}}{\text{Primary mass of the liposome}} \times 100 \quad (2)$$

Isolation of the unloaded drug from the targeted liposome containing CFB: After the drug loading, the encapsulated drug should be separated from the unloaded drug. The Sepharose-CL4B chromatographic column was used for this purpose. The drug-containing liposome passed through the column faster due to its larger size, and the drug passed later due to its smaller molecules. The presence of phospholipid in the blank samples was confirmed according to the color of the samples (orange). In fact, the concentration of phospholipid was measured, and the presence of phospholipid in the samples indicated the presence of the liposome. The orange color of the samples that came out of the column showed phospholipid-free samples, meaning that the drug was not loaded.

CFB drug release from liposome to non-targeted and targeted cells: For the investigation of the drug release process and simulation of drug release from the carrier in the *in-vivo* environment, sodium phosphate buffer at 37 and 42°C was used to establish the same conditions of pH and temperature. The release profile of CFB from the LECFB@AuNPs surface was obtained using dialysis; thus, 1 mM of the drug-containing liposome (10% (w/v) CFB drug and 1 mM liposome) was placed in a dialysis bag. Then, the dialysis bag was sterilized in an isolated environment. Sampling the environment dialysis was performed around the bag at specific times. The drug release at different times (30 and 60 min) and temperatures (37°C at p=7.4 for healthy cells and 42°C at pH=6 for cancer cells) was carried out using the drug calibration equation obtained in sodium phosphate buffer and the calculated release concentrations. The cumulative release rate of CFB can be calculated using the following equation:

$$\text{Cumulative release (\%)} = \frac{[(\text{Total CFB loaded on liposome}) - (\text{Unloaded CFB on liposome})]}{\text{Total CFB loaded on liposome}} \times 100 \quad (3)$$

Model of cancer

In the present work, two-photon excitation microscopy with fluorescence

Table 1. Loading conditions of the drug into the liposome.

S. No	Temperature (°C)	Drug:Lipid Ratio	Incubation Time (min)	Encapsulation Efficiency (%)
1	70	1:5	30	61.68 ± 2.99
2	70	1:5	60	68.07 ± 1.32
3	70	1:10	30	64.48 ± 2.82
4	70	1:10	60	63.55 ± 3.34
5	60	1:5	30	60.43 ± 1.04
6	60	1:5	60	72.38 ± 1.68
7	60	1:10	30	66.05 ± 1.32
8	60	1:10	60	62.45 ± 1.66

lifetime imaging (TPEM-FLIM) system (Jen Lab, Jena, Germany) was used to image the MCF-7 cancer cells. TPEM is an alternative to confocal and deconvolution microscopy that supplies distinct advantages for 3D imaging, and to produce an image based on the differences in the exponential decay rate of the fluorescence from a fluorescent sample, FLIM is a powerful tool. The basic study demonstrated that AuNPs can strengthen cellular imaging. It was demonstrated that TPEM-FLIM with using AuNPs can be a promising technique for biological labeling and imaging.

Cell culture

MCF-7 breast cancer cell was maintained in Roswell Park Memorial Institute medium (R^{PMI}-1640) consisting of 10% (v/v) fetal bovine serum, 300 U/mL penicillin, and 200 mg/L streptomycin. The culture of the cells as a monolayer was carried out with the density of 104 cells/cm² and maintained in tissue culture flasks (T-25). The incubation of the cultures was performed at 37°C with 5% CO₂.

Assessment of FR expression level

The expression of FR was evaluated by Western blotting analysis. A SDS-polyacrylamide gel (10%) was used to run cell lysates, and they were transferred to a nitrocellulose membrane that was blocked with Tween 20 (0.1%) in PBS and non-fat milk (5%) for 30 min, and then their incubation was performed overnight at 4°C with a dilution of anti-FR protein monoclonal antibody (1:2000). The detection of the antibody was done using a dilution of goat anti-mouse IgG-conjugated HRP (1:6000) and developed with Pierce ECL substrate.

Results and Discussion

FT-IR and Raman spectra of liposome-encapsulated CFB

The confirmation of borate formation was assessed by the spectra of FT-IR and Raman. Boron belongs to group III of the periodic table, and its isotopes are 11B (80.2%) and 10B (19.8%). Therefore, the content of 10B must be increased for synthesizing the active compositions. This process is called the "enrichment process", and this kind of enriched boron is commercially available. The major industrial usage of boron-containing compounds is in fire retardants. The results of FT-IR and Raman spectra showed that CFB could be applied in BNCT for the treatment of the tumor. Figure 2 shows FT-IR peaks for fructose, CFB, BA, and calcium carbonate. In the CFB spectrum, the fructose vibrational broadband attributed to the common functional and structural groups is found at 1100 cm⁻¹. A strong band and a band with a shoulder are respectively seen at 1444 cm⁻¹ and 1497 cm⁻¹ that correspond to the stretching of B-O of the external O-atoms. The stretching of B-O chain is confirmed with a very strong absorption peak at 1200 cm⁻¹. The peaks shown at 773 and 712 cm⁻¹ (shoulder), 739 and 643 cm⁻¹ (strong), and 688 cm⁻¹ (very strong) are related to the different deformational modes.

The analysis of Raman spectroscopic for CFB, fructose, BA, calcium carbonate was recorded at 532 nm, room temperature, and the exposure time of 10 min, and the results are presented in Figure 3. The spectrum of calcium carbonate is similar to the recorded spectrum for BA, and there exist no significant differences. The several peaks in the Raman spectrum of fructose can mainly be ascribed to the bending of O-H...O out-of-plane contribution. As for the Raman spectrum of CFB, the change in the position of the peak at 3314 cm⁻¹ is due to the B-O bond. According to the water crystallization of the structure, the weak peaks were broadened from 1602 to 1471 cm⁻¹.

Dynamic light scattering (DLS) and atomic force microscopy (AFM) of LECFB@AuNPs

Figures 4a and 4b show the DLS diagram of LECFB@AuNPs liposome with a size of around 240.9 nm, while the size of synthesized LECFB is 142.3 nm. Furthermore, Figures 5a and 5b are related to the two- and three-dimensional images of the distribution of the liposome nanocarrier before the drug loading, respectively. The agglomeration of the particles can be seen in the related figure, but this effect was highly eliminated due to the exact numerical calculations of the software, and the results are close to reality. It is

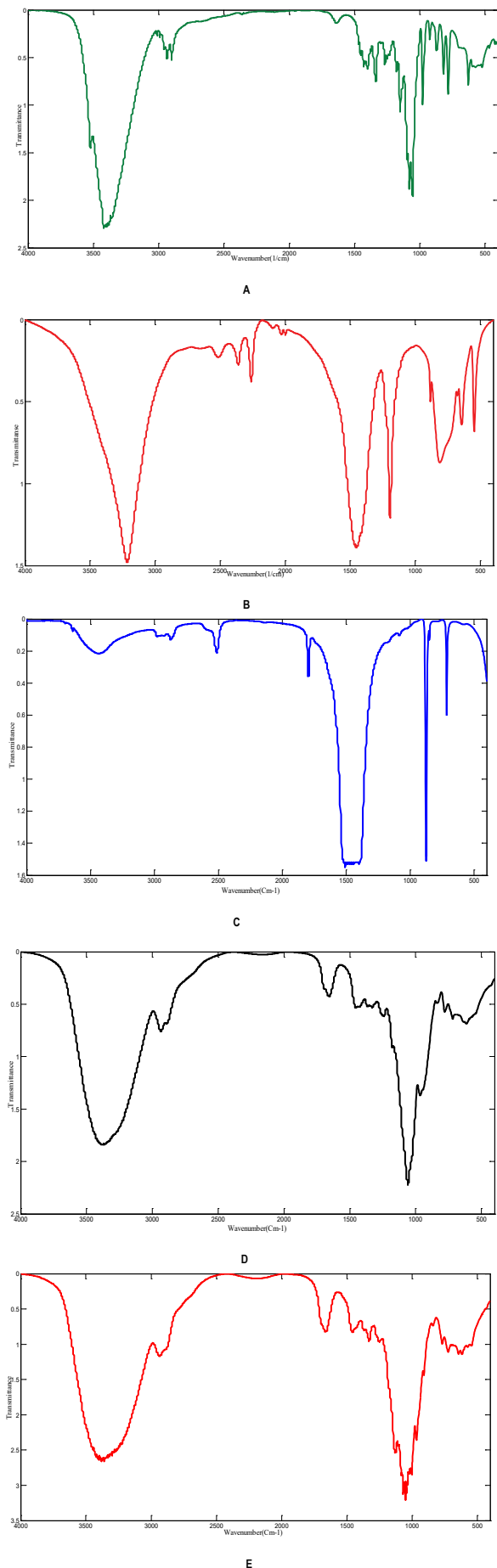


Figure 2. FT-IR spectra of (A) fructose, (B) boric acid, (C) calcium carbonate. CFB containing (D) 11B and (E) 10B.

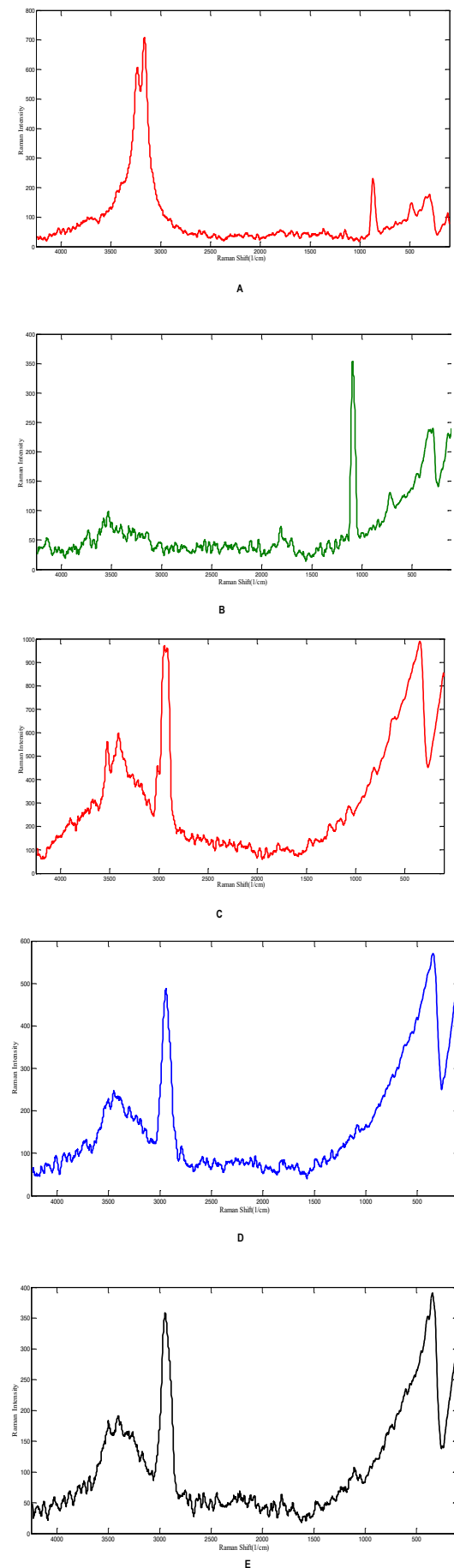
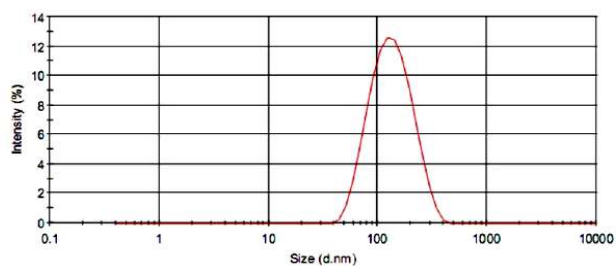


Figure 3. Raman spectra of (A) fructose, (B) boric acid, (C) calcium carbonate. CFB containing (D) 11B and (E) 10B.

	Diam. (nm)	% Intensity	Width (nm)
Z-Average (d.nm): 117.1	Peak 1: 142.3	100.0	61.94
Pdl: 0.191	Peak 2: 0.000	0.0	0.000
Intercept: 0.947	Peak 3: 0.000	0.0	0.000

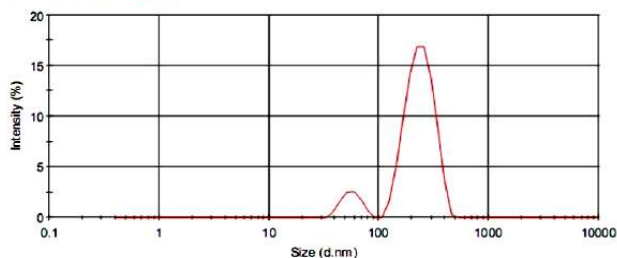
Result quality **Good**



A

	Diam. (nm)	% Intensity	Width (nm)
Z-Average (d.nm): 266.6	Peak 1: 240.9	90.1	66.65
Pdl: 0.472	Peak 2: 56.38	9.9	10.82
Intercept: 0.880	Peak 3: 0.000	0.0	0.000

Result quality **Good**



B

Figure 4. Size distribution of the liposome (A) Before and (B) After the drug loading.

also important to be noted that despite the agglomeration of the particles, it is possible to see the particles separately. Figures 5c and 5d are related to the two- and three-dimensional images of the distribution of liposome nanocarrier after the drug loading, respectively. As expected, the size of the liposome increases after the drug loading.

Calculation of CFB drug loading and release

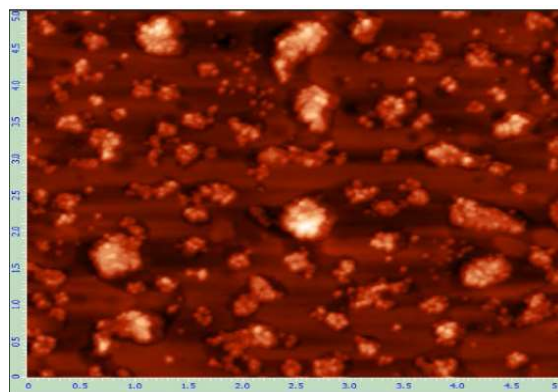
This experiment was done three times, and the results in Table 1 show that the highest drug loading was done within 1 h at 60 °C with the drug to lipid ratio of 1:5. The small values of deviation indicate uniformity in the drug content of the carrier. In addition, the quantity of the drug loading and encapsulation efficiency (over 72%) reveal that the drug and polymer (PEG) are two essential parameters for high drug loading, and such a result cannot be obtained without one of them.

Drug calibration curve

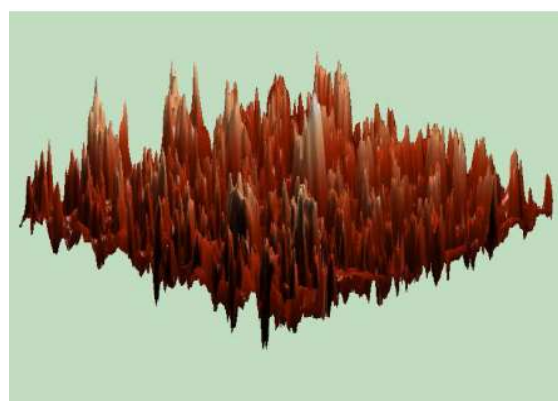
For the determination of the drug loading content, the drug concentration in the free form before loading (form (I)) and the amount of drug encapsulated into the liposome (form (II)) should be calculated. It can be noted that for plotting a release profile, the amount of drug that is not encapsulated into the liposome after loading (form (III)) should be also obtained. Due to the nature of CFB drug and according to the Beer-Lambert law, its concentration for the form (I) and (II) can be measured by using the flowmeter and spectrophotometer at 365 nm, respectively. Thus, certain dilutions of the CFB drug in sodium phosphate buffer were prepared, and their absorption was measured. Then, the standard calibration curves (Figures 6a and 6b) were obtained using the obtained results, and the equations of the calibration curves were as follows:

$$y=0.0097x + 0.0387 \rightarrow \text{Abs}=0.0097C + 0.0387 \quad (R^2=0.9963) \quad (1)$$

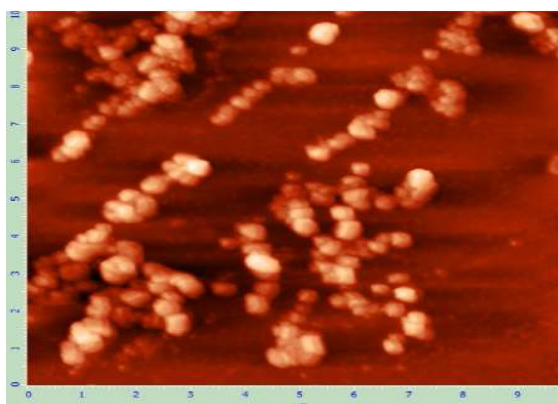
$$y=14.045x + 4.8143 \rightarrow \text{Abs}=14.045C + 4.8143 \quad (R^2=0.9873) \quad (2)$$



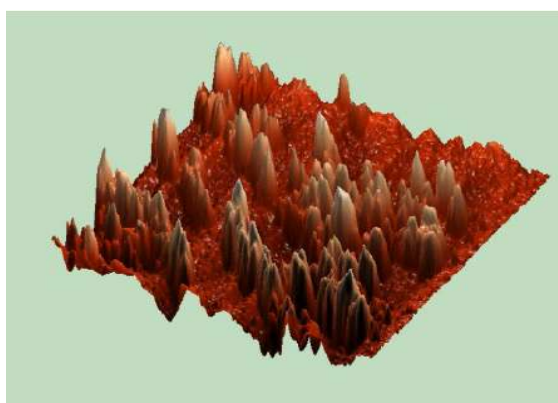
A



B



C



D

Figure 5. Two- and three-dimensional images of the liposome (A and B) before & (C and D) after drug loading.

The quantity of MCF-7 cancer cells obtained by a fluorescence microscope after 1, 3, 5, 7, 9, and 12 days of culture are shown in (Figure 7a), indicating that the cells are highly proliferated by using the method as long as the conditions of the cell culture are not changed. The transmission electron microscopy (TEM) images of the liposome in Figure 7b show that the drug-free liposome is spherical while the liposomes in the non-targeted and targeted cells are oval.

Evaluation of the drug release into the non-targeted and targeted cells

According to the results, the drug release rate in the first 24 h was less than 20% at two different pHs, and drug release was higher at pH=6 (Figure 8). Considering the statistical results (p-value <0.05), this difference is significant. Figure 9 shows a schematic of the entrance of the drug and the process of BNCT used in this investigation.

Investigation of the release patterns of the initial formulations

Three formulations (2, 6, and 7 named A, B, and C, respectively) were selected based on the rate of drug encapsulation into nanoliposomes, and the final formulation was selected according to the drug release pattern of the nanoliposomes obtained from the formulations. The release rate of the drug from the selected formulations at the temperatures of 37 and 42°C over a period of 48 h was calculated according to the drug calibration curve in phosphate buffer and its straight-line equation mentioned above, and the results are presented in Table 2.

As can be seen from the drug release results (Figures 10a and 10b), the charts have two exponential phases. A significant release is seen in the first phase due to the concentration gradient that occurred among the drug, inside the liposome, and the buffer. In the second phase, the slope of the drug release chart decreases; therefore, the highest rate of drug release can be obtained in the first 5 h, and then with a slower rate of the drug release, the

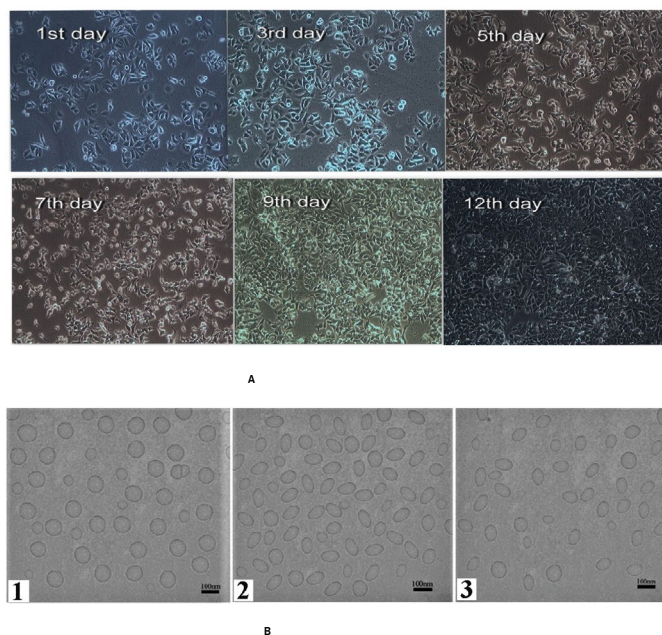


Figure 7. (A) Morphology of the cancer cells at different time intervals and (B) TEM of (1) drug-free liposome (2) liposome containing drug in the non-targeted cells, and (3) liposome containing drug in the targeted cells.

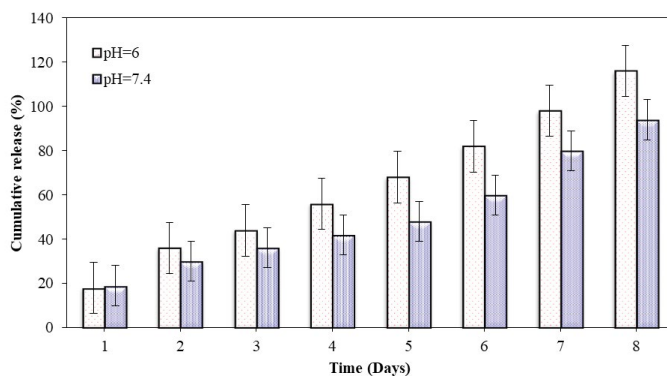
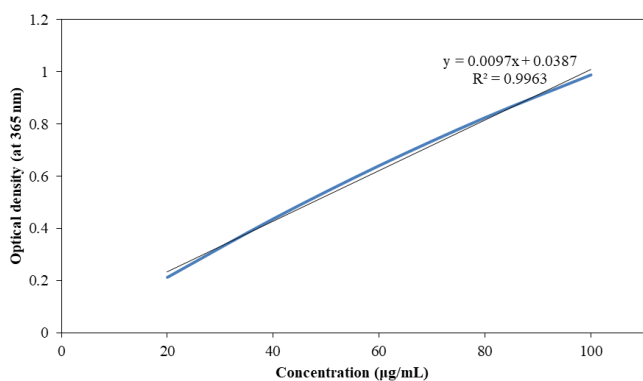
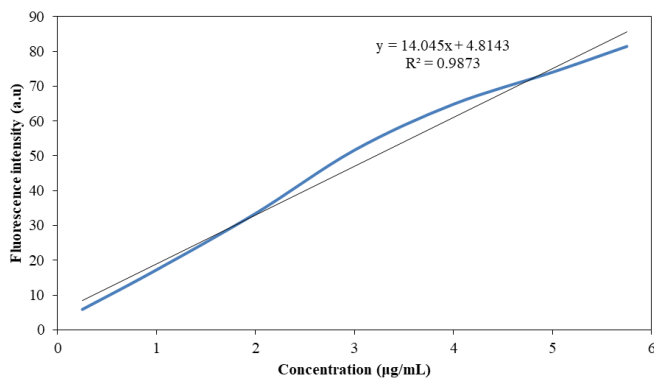


Figure 8. Drug release at pH=7.4 and pH=6.



A



B

Figure 6. Plots of (A) Optical density and (B) Fluorescence intensity at different concentrations of the drug.

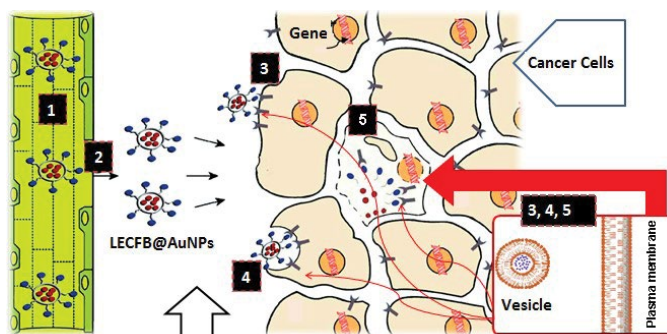
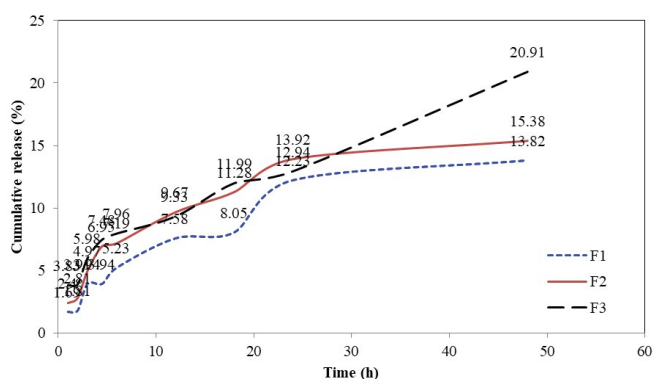


Figure 9. An overall schematic of the drug entrance and the process of BNCT.

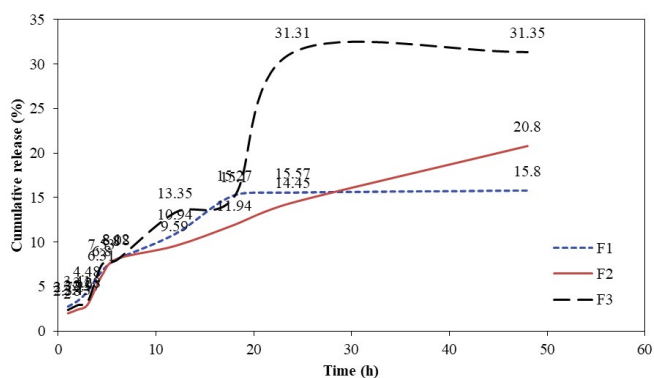
release rate is fixed, and a low slope can expose the cancer cells to the drug for a longer period. On the other hand, the higher release of the drug at 42°C and pH=6 ensures that the drug is delivered to the tumor site. Considering the two indicators of drug loading and release, formula B was selected as the final formulation, and it can keep the healthy cells out of the drug reach. The endocytosis of folate-conjugated LECFB@AuNPs in cancer cells that overexpress FA was significantly increased at pH=6 compared with pH=7.4. This emphasizes that the release of the drug has a low dependency on the pH of the medium. Nevertheless, the application of an agent is essential to supply a stimulus for an increase in the rate of release. The rate of release

Table 2. Results of the drug loading, encapsulation efficiency and size of liposome for (a) The selected liposomal formulations and (b) PEGylated liposome.

S. No.	Formula	Drug loading content (mg) (Mean ± SD)	Encapsulation efficiency (%) (Mean ± SD)	Size of liposome (nm)
a	A	1.445 ± 1.66	68.07 ± 1.32	138.82
	B	1.511 ± 0.026	72.38 ± 1.68	142.38
	C	1.398 ± 2.99	66.05 ± 1.32	136.35
b	B	1.511 ± 0.026	72.38 ± 1.68	142.38
	B-PEG	1.581 ± 0.029	75.75 ± 3.21	174.43



A



B

Figure 10. Drug release profile from liposome: (a) Healthy cell sample at 37 °C and pH=7.4 and (b) cancerous cell sample at 42 °C and pH=6.

can be enhanced by increasing temperature owing to the breakage of the π-π stacking interactions at a higher temperature. The results of this research indicate that the PEGylated liposomal system can be a suitable carrier because it possesses appropriate physicochemical properties; therefore, the chemical nature of the drug is not changed. In addition, it releases the entrapped drug at a continuous and controlled rate.

Investigation of PEGylation effect on the loading and release of CFB

Due to the effect of PEG on increasing the half-life and stability of lipid carriers, the effect of PEGylation on the loading rate and drug release was investigated after adding 5% PEG to the optimal formulation. According to the results, PEGylation improves the drug loading and increases the drug release rate. As can be seen in Table 2, the maximum release rates of the drug within 48 h are 24.43% for the healthy cells and 26.81% for the cancer cells. PEGylated liposomal carrier improves 0.07 mg of the drug loading content, and the amounts of the drug release from PEGylated formulation at 37 and 42°C are respectively 8.89 and 5.78% more than those obtained by formula B (Figures 11a and 11b). In the present study, the results demonstrated that the total amount of CFB drug was found to be 1.511 ± 0.026. According to the total

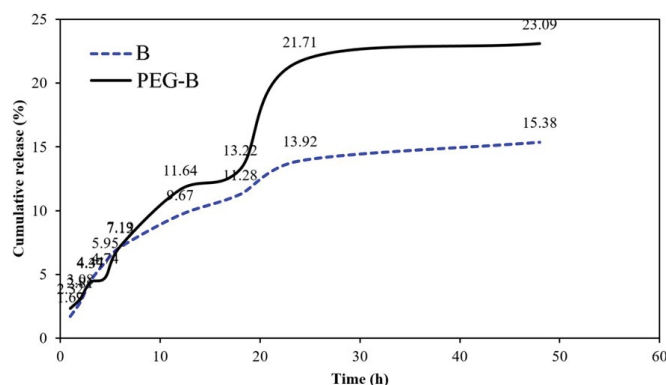
quantity of drug loading, the encapsulation efficiency was calculated, and the results are demonstrated in Table 2.

Imaging of cancer cells by fluorescence lifetime imaging

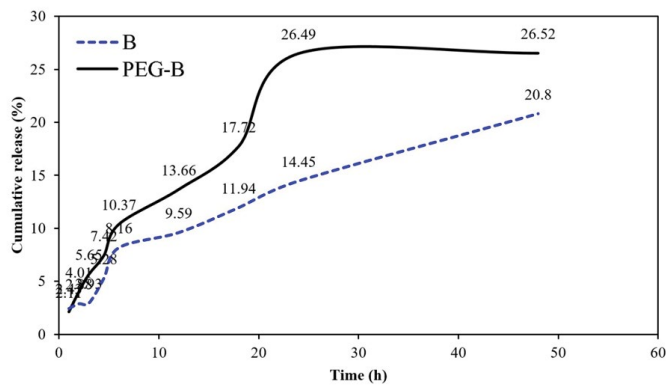
AuNPs are used as optical probes in biological imaging according to their unique properties in the field of labeling tools. AuNPs conjugated with LECFB can convert optical storage to heat energy through light absorption. The bilayer membrane of lipid can be disrupted at higher temperatures, accordingly, CFB is simultaneously released. In addition, the temperature-induced phase transition significantly affects the fluidity and structure of the bilayer membrane of lipid that further affects the release of the drug. The release of the drug is prevented in physiological environments owing to physiological temperature (37°C) that is lower than the required temperature for the transition of phosphatidylcholine (as the main structural component of liposomes), while a temperature higher than the transition temperature (42°C) increases the release of the drug via the bilayer membrane disruption of lipid.

Using FLIM at 750 nm, the intensity and FLIM images of MCF-7 cells were recorded according to the distinct fluorescence lifetime difference between the cancer cells conjugated with optical probes (herein, AuNPs) and healthy cells. Figure 12 shows that AuNPs have tunable optical and electronic properties and detect red fluorescence due to ultraviolet radiation. The predetermined concentration of 10B was 20-35 µg of 10B/g tumor. The uptake of boron atoms in MCF-7 cancer cells using FR-bonded LECFB@AuNPs could be 5-10-fold more than that obtained with LECFB@AuNPs that could be related to the multivalent nature of the FR-FA binding. The attachment of a broad range of liposomes to folate has been confirmed to be highly efficient as targeted delivery systems.

Figures 13a and 13b show the fluorescence imaging of the cancer cell with the drug-free liposome and drug-containing liposome, respectively. Columns



A



B

Figure 11. Drug release profile of the optimal and PEGylated formulation: (A) Healthy cells at 37°C and pH=7.4 and (B) cancer cells at 42°C and pH=6.

(1), (2), and (3) represent the DAPI-colored core under the blue filter (a1 and b1), Dil-painted system under the green filter (a2 and b2), and the images without filter (a3 and b3), respectively. By comparing the images, the entrance of the drug into the cancer cells can be confirmed.

It should be noted that the retention time of AuNPs in the targeted cells should be increased, and their accumulation in the non-targeted cells should be reduced. AuNPs were utilized for the sensitization of the cancer cells and increasing the absorption of the dose that by the cells. The uptake of AuNPs in the cells can be increased by active targeting (neutron radiation), while it has a small influence on the healthy cells. As displayed in Figure 14, LECFB@

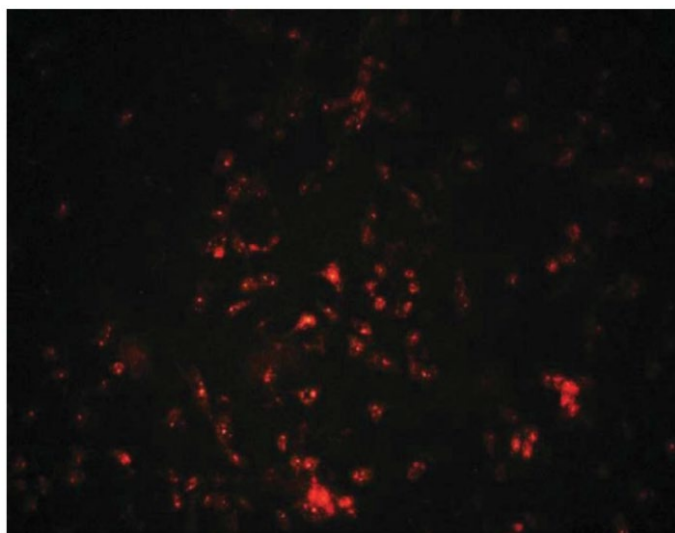


Figure 12. Fluorescence microscopy of MCF-7 cancer cells treated with LECFB@AuNPs.

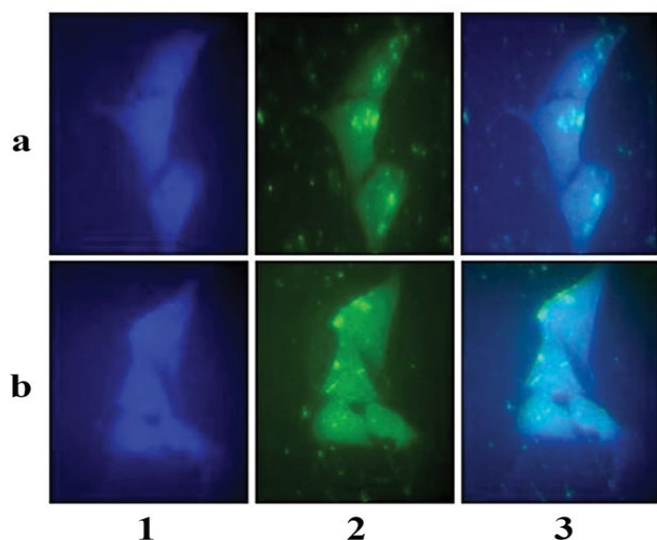


Figure 13. Fluorescence imaging of MCF-7 cancer cells treated with (a) drug-free liposome and (b) drug-containing liposome.

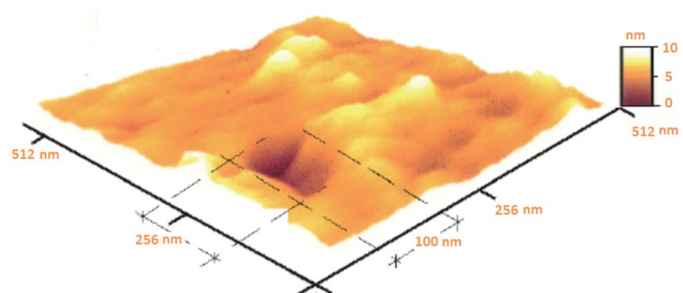


Figure 14. AFM of MCF-7 cancer cells treated with LECFB@AuNPs.

AuNPs could absorb the neutron radiation in a large surface of the tumor cells, and the dark area shows unreceived LECFB@AuNPs.

Conclusion

BNCT is one of the highly selective types of radiation treatment, in which the irradiation of non-radioactive ^{10}B is carried out with low energy thermal neutrons for the destruction of cancer cells through $^{10}\text{B}(n,\alpha)^7\text{Li}$ reaction. In this research, the ability of LECFB was designed as a biological product and boron carrier agent for the treatment of MCF-7 cancer cells by the BNCT method. AuNPs as the optical probe in the form of LECFB@AuNPs core-shell nanostructure were selected in order to perform fluorescence lifetime imaging. The DLS and AFM results demonstrated a slight agglomeration of the particles and an increase in the size of the liposome after the drug loading up to 142.3 nm. As the optimum encapsulation efficiency was 72.38 ± 1.68 at the temperature of 60°C , an attractive approach could be suggested to increase the internalization and accumulation of the drug in the targeted cells. The maximum release rate of the drug within 48 h was 24.43% for the healthy cells and 26.81% for the cancer cells. PEGylated liposomal carrier improved 0.07 mg of the drug loading content, and the amounts of drug release were 8.89 and 5.78% in the PEGylated formulation at 37 and 42°C , respectively. Due to the appropriate physicochemical properties of LECFB@AuNPs, it does not cause any change in the chemical nature of the drug, accordingly, it can be a suitable carrier for CFB. A discriminate imaging difference was shown between cancer cells conjugated with AuNPs and healthy cells that were a result of the tunable optical and electronic properties of AuNPs. In conclusion, the successful results of this study provide a reference for the treatment of MCF-7 cancer cells with the BNCT method.

Acknowledgements

The authors are thankful for the financial support received from Babol Noshirvani University of Technology.

Conflict of Interest

None.

References

- Moss, Raymond L. "Critical review, with an optimistic outlook, on Boron Neutron Capture Therapy (BNCT)." *Appl Radiat Isot* 88 (2014): 2-11.
- Farhood, Bagher, Hadi Samadian, Mahdi Ghorbani and Seyed Salman Zakariaee, et al. "Physical, dosimetric and clinical aspects and delivery systems in neutron capture therapy" *Rep Pract Oncol Radiother* 23 (2018): 462-473.
- Hamoudeh, Misara, Muhammad Anas Kamleh, Roudayna Diab and Hatem Fessi. "Radionuclides delivery systems for nuclear imaging and radiotherapy of cancer" *Adv Drug Deliv Rev* 60 (2008): 1329-1346.
- Nakamura, Hiroyuki. "Liposomal Boron delivery for neutron capture therapy" *Methods Enzymol* 465 (2009): 179-208.
- Shah, Muhammad Raza, Muhammad Imran and Shafi Ullah. "Nanocarriers for cancer diagnosis and targeted chemotherapy." Elsevier (2019).
- Lee, Woonghee, Swarbhanu Sarkar, Heesu Ahn, Jung Young Kim, et al. "PEGylated liposome encapsulating nido-carborane showed significant tumor suppression in boron neutron capture therapy (BNCT)" *Biochem Biophys Res Commun* 522 (2020) 669-675.
- Nakamura, H., M. Ueno, H. S. Ban and K. Nakai, et al. "Development of boron nanocapsules for neutron capture therapy." *Appl Radiat Isot* 67 (2009): S84-S87.
- Gifford, Ian, Wyatt Vreeland, Slavica Grdanovska and Eric Burgett, et al. "Liposome-based delivery of a boron-containing cholesteryl ester for high-LET particle-induced damage of prostate cancer cells: a boron neutron capture therapy study" *Int J Radiat Biol* 90 (2014) 480-485.
- Yanagie, H., H. Kobayashi, Y. Takeda and I. Yoshizaki et al. "Inhibition of growth of

- human breast cancer cells in culture by neutron capture using liposomes containing ^{10}B " *Biomed Pharmacother* 56 (2002): 93-99.
10. Luderer, Micah John, Barbara Muz, Kinan Allhalk and Jennifer Sun, et al. "Thermal Sensitive Liposomes Improve Delivery of Boronated Agents for Boron Neutron Capture Therapy" *Pharm Res* 36 (2019): 144.
 11. Rotaru, P., R. Scorei, Ana Hărăbor and M.D. Dumitru. "Thermal analysis of a calcium fructoborate sample." *Thermochimica Acta* 506 (2010): 8-13.
 12. Białek-Pietras, Magdalena, Agnieszka B. Olejniczak, Shoji Tachikawa and Hiroyuki Nakamura, et al. "Towards new boron carriers for boron neutron capture therapy: Metallacarboranes bearing cobalt, iron and chromium and their cholesterol conjugates" *Bioorg Med Chem* 21(5) (2013): 1136-1142.
 13. Rajani, Chitra, Pooja Borisa, Tukaram Karanwad and Yogeshwari Borade, et al. "Cancer-targeted chemotherapy: Emerging role of the folate anchored dendrimer as drug delivery nanocarrier" *Pharmaceutical Appl Dendrimers* (2020): 151-198.
 14. Şener, Sevil, A. Tahir Bayrac, B. Bilgenur Şener and Cem Tozlu, et al. "Synthesis, characterization, and DFT study of novel metallo phthalocyanines with four carboranyl clusters as photosensitisers for the photodynamic therapy of breast cancer cells" *Eur J Pharm Sci* 129 (2019): 124-131.
 15. Valliant, John F and Paul Schaffer. "A new approach for the synthesis of isonitrile carborane derivatives.: Ligands for metal based boron neutron capture therapy (BNCT) and boron neutron capture synovectomy (BNCS) agents" *J Inorg Biochem* 85 (2001): 43-51.
 16. Yanagie, Hironobu, Koichi Ogura, Toshio Matsumoto and Masazumi Eriguchi, et al. "Neutron capture autoradiographic determination of ^{10}B distributions and concentrations in biological samples for boron neutron capture therapy" *Nucl Instrum Methods Phys Res* 424(1) (1999) 122-128.
 17. Yanagië, Hironobu, Koichi Ogura, Kenji Takagi and Kazuo Maruyama, et al. "Accumulation of boron compounds to tumor with polyethylene-glycol binding liposome by using neutron capture autoradiography" *Appl Radiat Isot* 61 (2004): 639-646.
 18. Carvalho, Andreia, Alexandra R. Fernandes and Pedro V. Baptista, et al. "Chapter 10 - Nanoparticles as Delivery Systems in Cancer Therapy: Focus on Gold Nanoparticles and Drugs" *Appl Target Nano Drugs Deliv Sys* (2019) 257-295.
 19. Barth, Rolf F., Peng Mi and Weilian Yang. "Boron delivery agents for neutron capture therapy of cancer" *Cancer Commun (Lond)* 38 (2018): 1-15.
 20. Hu, Kuan, Zhimin Yang, Lingling Zhang and Lin Xie, et al. "Boron agents for neutron capture therapy" *Coord Chem Rev* 405 (2020) 213139.
 21. Farran, Batoul, Raquel Carvalho Montenegro, Prameswari Kasa and Eluri Pavitra, et al. "Folate-conjugated nanovehicles: Strategies for cancer therapy" *Mater Sci Eng C Mater Biol Appl* 107 (2020) 110341.
 22. Gosselin, Michael A and Robert J. Lee. "Folate receptor-targeted liposomes as vectors for therapeutic agents" *Biotechnol Annu Rev* 8 (2002) 103-131.
 23. Ito, Y., Y. Kimura, T. Shimahara and Y. Ariyoshi, et al. "Disposition of TF-PEG-Liposome-BSH in tumor-bearing mice" *Appl Radiat Isot* 67 (2009) S109-S110.
 24. Niidome, Takuro, Akira Ohga, Yasuyuki Akiyama, Kazuto Watanabe, et al. "Controlled release of PEG chain from gold nanorods: Targeted delivery to tumor" *Bioorg Med Chem* 18 (2010): 4453-4458.
 25. Yanagie, H., K. Maruyama, T. Takizawa and K. Ogura, et al. "Tumor growth suppression by boron neutron capture therapy with ^{10}B entrapped PEG-liposome in pancreatic cancer model in vivo" *Eur J Cancer* 35 (1999): S186-S187.
 26. Heber, Elisa M., Peter J. Kueffer, Mark W. Lee and M. Frederick Hawthorne, et al. "Boron delivery with liposomes for boron neutron capture therapy (BNCT): biodistribution studies in an experimental model of oral cancer demonstrating therapeutic potential." *Radiat Environ Biophys* 51 (2012): 195-204.
 27. Barth, Rolf F. "Boron neutron capture therapy at the crossroads: challenges and opportunities." *Appl Radiat Isot* 67 (2009): S3-S6.
 28. Chen, Wei, Samir C. Mehta, and D. Robert Lu. "Selective boron drug delivery to brain tumors for boron neutron capture therapy." *Adv Drug Deliv Rev* 26 (1997): 231-247.
 29. Luderer, Micah John, Pilar De La Puente, and Abdel Kareem Azab. "Advancements in tumor targeting strategies for boron neutron capture therapy." *Pharm Res* 32 (2015): 2824-2836.
 30. Martini, Silvia, Sandra Ristori, Amaranta Pucci and Claudia Bonechi, et al. "Boronphenylalanine insertion in cationic liposomes for boron neutron capture therapy." *Biophys Chem* 111 (2004): 27-34.
 31. Olusanya, Temidayo O.B., Gianpiero Calabrese, Dimitrios G. Fatouros and John Tsiouklis, et al. "Liposome formulations of o-carborane for the boron neutron capture therapy of cancer." *Biophys Chem* 247 (2019): 25-33.
 32. Huang, Lin-Chiang Sherlock, Wen-Yuan Hsieh, Jiun-Yu Chen and Su-Chin Huang, et al. "Drug delivery system design and development for boron neutron capture therapy on cancer treatment." *Appl Radiat Isot* 88 (2014): 89-93.
 33. Ueno, Manabu, Hyun Seung Ban, Kei Nakai and Ryu Inomata, et al. "Dodecaborate lipid liposomes as new vehicles for boron delivery system of neutron capture therapy." *Bioorg Med Chem* 18 (2010): 3059-3065.
 34. Gadan, M.A., Sara Josefina González, M. Batalla and M.S. Olivera, et al. "Application of BNCT to the treatment of HER2+ breast cancer recurrences: Research and developments in Argentina." *Appl Radiat Isot* 104 (2015): 155-159.
 35. Marone, Palma Ann, James T. Heimbach, Boris Nemzer, and John M. Hunter. "Subchronic and genetic safety evaluation of a calcium fructoborate in rats." *Food Chem Toxicol* 95 (2016): 75-88.
 36. Smoum, R and M. Srebnik. "Boronated saccharides: Potential applications." *Studies Inorg Chem* 22 (2005): 391.
 37. Maruyama, Kazuo. "Intracellular targeting delivery of liposomal drugs to solid tumors based on EPR effects." *Adv Drug Deliv Rev* 63 (2011): 161-169.
 38. Maruyama, Kazuo, Osamu Ishida, Satoshi Kasaoka and Tomoko Takizawa, et al. "Intracellular targeting of sodium mercaptoundecahydrododecaborate (BSH) to solid tumors by transferrin-PEG liposomes, for boron neutron-capture therapy (BNCT)." *J Control Release* 98 (2004): 195-207.
 39. Yanagie, H., K. Maruyama, T. Takizawa and O. Ishida, et al. "Application of boron-entrapped stealth liposomes to inhibition of growth of tumour cells in the in vivo boron neutron-capture therapy model." *Biomed Pharmacother* 60 (2006): 43-50.
 40. Bhuvana, Mohanlal and Venkataraman Dharuman. "Influence of alkane chain lengths and head groups on tethering of liposome-gold nanoparticle on gold surface for electrochemical DNA sensing and gene delivery." *Sens Actuators B Chem* 223 (2016): 157-165.
 41. Miao, Yanqin, Peng Tao, Long Gao and Xiangling Li, et al. "Highly efficient chlorine functionalized blue iridium (III) phosphors for blue and white phosphorescent organic light-emitting diodes with the external quantum efficiency exceeding 20%." *J Mater Chem C* 6 (2018): 6656-6665.
 42. Raza, Muhammad, Muhammad Imran and Shafi Ullah, "Nanotargeted radiopharmaceuticals for cancer diagnosis and treatment" Elsevier (2019): 247-266
 43. Alberti, Diego, Nicoletta Protti, Antonio Toppino and Annamaria Deagostino, et al. "A theranostic approach based on the use of a dual boron/Gd agent to improve the efficacy of Boron Neutron Capture Therapy in the lung cancer treatment." *Nanomed: Nanotechnol Biol Med* 11 (2015): 741-750.
 44. Asano, Ryuji, Amon Nagami, Yuki Fukumoto and Kaori Miura, et al. "Synthesis and biological evaluation of new boron-containing chlorin derivatives as agents for both photodynamic therapy and boron neutron capture therapy of cancer." *Bioorg Med Chem Lett* 24 (2014): 1339-1343.
 45. Dewi, Novriana, Hironobu Yanagie, Haito Zhu and Kazuyuki Demachi, et al. "Tumor growth suppression by gadolinium-neutron capture therapy using gadolinium-entrapped liposome as gadolinium delivery agent." *Biomed Pharmacother* 67 (2013): 451-457.
 46. Feakes, Debra A., Jennifer K. Spinler, and Fred R. Harris. "Synthesis of boron-containing cholesterol derivatives for incorporation into unilamellar liposomes and evaluation as potential agents for BNCT." *Tetrahedron* 55 (1999): 11177-11186.
 47. Halfon, Sh, A. Arenshtam, D. Kijel and M. Paul, et al. "Demonstration of a high-intensity neutron source based on a liquid-lithium target for Accelerator based Boron Neutron Capture Therapy." *Appl Radiat Isot* 106 (2015): 57-62.
 48. Heber, Elisa M., M. Frederick Hawthorne, Peter J. Kueffer and Marcela A. Garabalino, et al. "Therapeutic efficacy of boron neutron capture therapy mediated by boron-rich liposomes for oral cancer in the hamster cheek pouch model." *Proc Natl Acad Sci* 111 (2014): 16077-16081.
 49. Singh, Ajay, Byung Kyu Kim, Yuri Mackeyev and Parham Rohani, et al. "Boron-nanoparticle-loaded folic-acid-functionalized liposomes to achieve optimum boron concentration for boron neutron capture therapy of cancer." *J Biomed Nanotechnol* 15 (2019): 1714-1723.

50. Pirouz, F., G. Najafpour, M. Jahanshahia, and M. Sharifzadeh Baei. "Plant-based calcium fructoborate as boron-carrying nanoparticles for neutron cancer therapy." *Int J Eng* 32 (2019): 460-466.
51. Sadeghi, Meisam, Mohsen Jahanshahi, and Hamedreza Javadian. "Synthesis and characterization of a novel $\text{Fe}_3\text{O}_4\text{-SiO}_2\text{@}$ Gold core-shell biocompatible magnetic nanoparticles for biological and medical applications." *J Nanomed Res* 4 (2019): 193-203.

How to cite this article: Sadeghi, Meisam Zahra Moghimifar and Hamedreza Javadian. "Boron Neutron Capture Therapy of MCF-7 Breast Cancer Cells by Using Calcium Fructoborate@Au Nanoparticles Drug Encapsulated in Liposomal Nanocarriers: In-vitro Experimental Investigation." *J Nucl Med Radiat Ther* 13 (2022): 496.